SSC20-VI-01

A Foldable, Compact and Lightweight Solar Array Substrate with Large Deployed Wingspan for Small Spacecraft

Calvin Kee, Michael Marley, Mark Bryant, Erich Schulze, Kenneth Harclerode, Clint Apland, James Leary
Johns Hopkins Applied Physics Laboratory
11100 Johns Hopkins Road, Laurel, Maryland 20723; (240) 228 4129
calvin.kee@jhuapl.edu

ABSTRACT

A solar array (SA) mechanical subsystem made of thin and lightweight substrates was developed, built and tested for a small spacecraft. The SA is compactly foldable and deployable to a length of approximately five times the width of the spacecraft. It has miniature hinges and latches, and deploys freely without dampers and synchronizing mechanisms. The solar cell interconnect harness consists of thin, laminated flexible circuits, and the substrates feature a syntactic foam core exposed to large temperature extremes. This developmental technology, currently at TRL 6, when completely proven out, would be viable for small satellites and would enable missions in the Express-class. The Express-class (or Express) refers to satellites in the range of 25 kg to 100 kg that are positioned in the gap between 12U CubeSats and small ESPA-class spacecraft.

Cornerstones of the SA development were compact packaging, deployment dynamic simulation, and hinge-latch tuning for dynamics and lock-up loads. Dynamic deployment simulations were modeled in Adams to observe the behavior of the unfolding array, to size the hinge springs and to monitor the lockup loads at the substrate to hinge interfaces. Extensive substrate mechanical and thermal tests were conducted to verify the substrate's structural capability and dimensional stability in its operating environment. Thermal tests were carried out to observe the effect of mismatching coefficients of thermal expansion between the adhered flexible laminated interconnect circuits and the substrate. Gravity-negated wing deployment tests were performed at temperature limits and in vacuum to verify the overall design intent of the deployment. The stowed wing was vibration tested to verify its structural capabilities under launch environments, and then deployment tested again to demonstrate that the array as a mechanism was unaffected by launch loads.

Mechanically, the Express SA substrate assembly has been advanced in its development and proven out as a structure and mechanism. Further development of the electrical power system is necessary, and additional testing for mechanical and thermal interactions of the solar cells with the overall SA substrate will need to be done. This SA subsystem would be an essential expansion to the Express hardware developed by The Applied Physics Laboratory (APL) for the advancement and enablement of Express-class missions.

BACKGROUND

There is a need to develop the capability for substantial electrical power in the Express class of satellites to boost mission objectives and durations to beyond earth orbits and beyond short lifespans. In order to support these large amounts of power, there has to be a large area for sun exposure. For the Express, the large array will need to be folded away compactly within the Express' volume while leaving a significant portion of that volume for packaging spacecraft structure and subsystems. The large sun exposure criteria was fulfilled by a conventional Z-fold array that was developed to be thin, lightweight, compactly folded (stowed), and unfolded (deployed) to an augmented area that is five times the footprint of the stowed configuration. The stowed array was limited to the width and height of the Express for packaging and launch provisions. The stowed array stack was also limited such that the overall Express was within a 16-in square footprint.

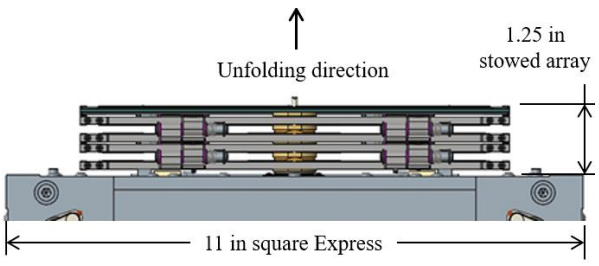

Figure 1: Compactly Stowed Array on One Side of an Express-Class Spacecraft

Because of the compact packaging, thin-panel substrates were the apparent choice for this array. Standard solid

carbon fiber (CF) laminates could be used, but instead, a substrate with thin CF facesheets and a 0.040-in thick syntactic foam (SF) core was fabricated to produce a lightweight structure that is as thick as a solid CF laminate, and that has 1.6x lower mass moment of inertia than the solid CF laminate, while meeting deployed stiffness requirements.

The array consists of five of these CF-SF-CF laminated substrates. It has five hinge lines, folds in a zig-zag pattern, and when deployed is approximately 7.5 feet long. There could be up to four of these arrays on the Express spacecraft.

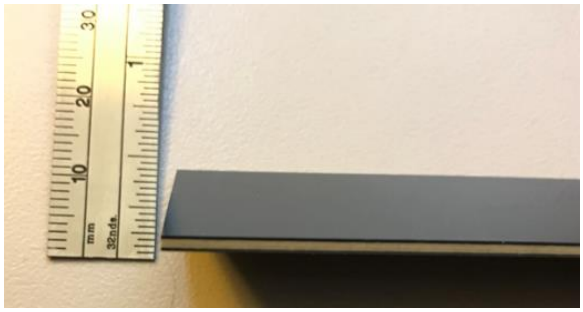

Figure 2: The CF-SF-CF Laminate is 0.060 in Thick

The CF facesheets are made of 4 plies of uniaxial M55J/RS3C fiber preimpregnated with cyanate-ester resin laid up in a quasi-isotropic configuration [0/45/90/-45] that builds up to 0.010 in. The syntactic foam is a cyanate-ester-based material from Tencate, with the trade name SF5 and a nominal thickness of 0.040 in. The substrate has the following layup configuration: [0/45/90/-45]CF – SF – [-45/90/45/0]CF. The layup is cured at 350°F for 2 hours to form the laminate.

SUBSTRATE MECHANICAL TESTING AND SUPPORTING ANALYSES

There is little published data on the mechanical properties of the CF-SF laminate, and in a need to understand the behavior and to prove the structural viability of this substrate for this particular application, a series of mechanical tests was conducted. The mechanical test samples were all preconditioned with temperature cycling of -95 °C to 105 °C for 6 cycles in nitrogen.

In-Plane Tension

The in-plane tension test was performed with 6 laminate samples according to ASTM D3039, with the 0-degree ply direction corresponding to the pull direction. Mechanical properties obtained were tensile ultimate strength, tensile elastic modulus, and Poisson's ratio.

In-Plane Compression

The in-plane compression test was performed with 6 laminate samples according to ASTM D695, with the 0-degree ply direction corresponding to the push direction. Mechanical properties obtained were compressive ultimate strength and compressive elastic modulus.

Flatwise Tension

The flatwise tension test was performed with 6 laminate samples according to ASTM D7291 to determine core-to-facesheet interface tensile strength and inter-laminar tensile strength.

Short-Beam Shear

The short-beam shear test was performed with 6 laminate samples according to ASTM D2344 for inter-laminar shear strength.

Flexural

The flexural, 3-point bending test was performed according to ASTM D7264 to determine flexural properties such as flexural strength, load-deflection and flexural modulus. The 0-degree ply direction of the laminate was aligned with the long dimension of the 3-point bending sample. For this test, there were 3 thermal conditions:

- as fabricated without temperature cycling, 6 samples
- 6 cycles of -95 °C to 105 °C, 6 samples
- 6 cycles of -150 °C to 173 °C, 6 samples

The 3-point bending test was a good way to subject the laminate in both tension and compression and to determine the effect of temperature on the flexural properties, depending on the expected thermal environment and the expected mechanical loading of the substrate in orbit.

Cantilevered

The cantilevered test was a custom test to determine the substrate bending capability during hinge lockup at wing deployment. The measured property was the ultimate bending strength of the laminate with one end fixed, as in a hinge bracket, and the free end being the loaded end.

The results of the substrate mechanical testing are summarized in Table 1.

Table 1: B-Basis Results of Mechanical Testing

Test Description	ASTM	Ultimate Load (lb)	Ultimate Strength (ksi)	Elastic Modulus (Mpsi)
In-plane tension	D3039	-	26.2	5.29
In-plane compression	D695	-	15.5	4.65
Flatwise tension	D7291	-	1.91*	-
Shortbeam shear	D2344	-	4.13	-
Cantilevered	-	11.6	-	-
Flexural 3-point bend, No TC	D7264	-	-	11.5
Flexural 3-point bend, 6x TC -95°C to 105°C	D7264	-	-	10.7
Flexural 3-point bend, 6x TC -150°C to 173°C	D7264	-	-	10.8
* Minimum value; the standard deviation was large leading to a coefficient of variation greater than 10%				

While mechanical strength testing was important, determining the structural integrity of the substrate in environments with large temperature differentials was of more significance. The substrate consisted of two materials with highly mismatched thermal expansion coefficients, and although the core's modulus of elasticity was 2 orders of magnitude lower than that of the facesheet, there was a concern of how the laminae would interact and affect the integrity and dimensional stability of the laminate in large temperature excursions. Three thermal-distortion mechanical tests were carried out as follows.

Liquid Nitrogen Soak and Visual Inspection

A long sample of the substrate, approximately 18" x 1", was soaked for 1 minute in liquid nitrogen, which has a temperature of -198°C. After the soak, the sample was visually inspected and no delamination or core tear-away was observed.

Tap Test

The objective of the tap test was to observe any change in resonant frequencies of the substrate after exposure to the different temperature ranges, which were

- as fabricated without temperature cycling
- 6 cycles of -95 °C to 105 °C
- 6 cycles of -150 °C to 173 °C.

After each temperature condition, the substrate laminate measuring 8" x 17.5" was hung vertically from 2 of its corners. Accelerometers (accels) were mounted onto the laminate at 3 locations and the laminate was then tapped at 7 locations as indicated in Figure 3. Transient time-history plots of the events were captured and converted to frequency response formats.

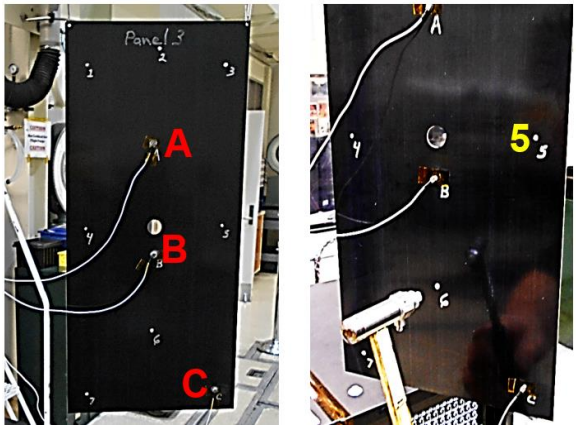

Figure 3: Laminate was Instrumented and Tapped to Measure Frequency Responses

From the results of the tap test (Figure 4 and Figure 5), it was found that there was no significant change in resonant frequencies of the laminate after exposure to 3 temperature conditions. This demonstrated that there was no degradation of the laminate structure due to large temperature changes in the substrate's environment.

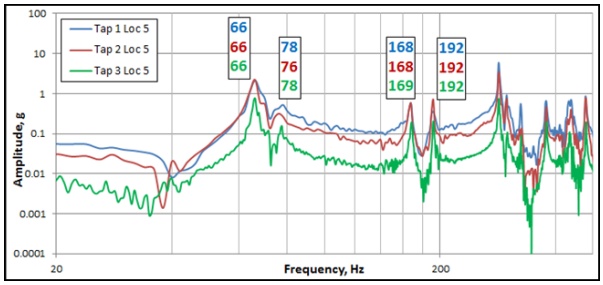

Figure 4: Responses at Accel B, Tapped Location 5

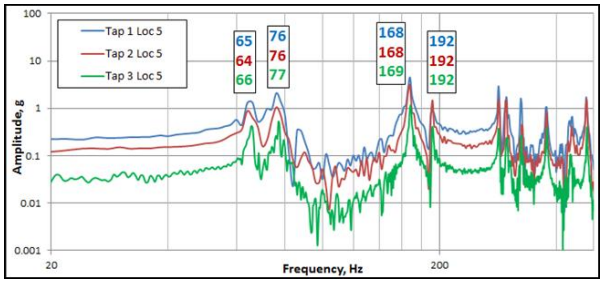

Figure 5: Responses at Accel C, Tapped Location 5

3-Point Bend

This test was described in the *Flexural* mechanical testing above. The secondary objective of that test was to observe any change in the flexural properties of the substrate laminate with exposure to different ranges of temperatures. It was expected that any thermal exposure on a carbon fiber laminate would weaken the resin matrix a small amount, and this weakening would

saturate with prolonged temperature exposure. In this test, the flexural modulus reduced by 8.7% from the as-fabricated, unexposed state, to the 1st temperature condition. In the 2nd temperature condition, a reduction of 7.9% was observed in the flexural modulus. The moduli were determined to be 11.6 Mpsi and 11.7 Mpsi, respectively, for the 1st and 2nd temperature conditions, which showed that there were no strength and stiffness changes in the laminate structure, demonstrating that it would hold up in the thermal environments.

Shear Lag Model

The stress analyses to support the test observations of thermal distortion on this laminate was based on Volkersen's shear lag model.[3] Volkersen's shear lag equations were originally modeled for a bonded lap joint, but the syntactic foam in this laminate had mechanical properties similar to adhesive and in this case the equations were appropriate. The shear lag theory was based on a tension load on the adherends and the adhesive experiences only shear. This model assumed the adherends were elastic, and therefore the shear stress distribution was hyperbolic, peaking at the edge of the joint, and low in the interior. In the case where the laminate was being affected by temperature, the coefficient of thermal expansion (CTE) and in-plane thermal distortion would be the tensile loading. The calculations were supplemented with finite element analyses (FEA).

The shear lag equations substituted with thermally induced tension forces are as follows:

$$C = \sqrt{\frac{G_2}{t_2}\left[\frac{1}{E_1 t_1} + \frac{1}{E_3 t_3}\right]} \qquad (1)$$

$$\tau(x) = \frac{G_2}{C t_2}\left[(\alpha_3 - \alpha_1)\Delta T \frac{\sinh(Cx)}{\cosh(C\,L/2)}\right] \qquad (2)$$

where subscripts $_1$, $_2$ and $_3$ refer to the top adherend, the adhesive and the bottom adherend, respectively; G, E and t are the shear modulus, elastic modulus and the thickness of each component in the bond joint; x is the location along the bond joint and L is the length of the bond (in this case, it is the length of the laminate); τ is the shear stress in the adhesive (the syntactic foam core), α is the CTE of the adherends, and ΔT refers to the temperature differential.

For the thermal distortion of a laminate with a syntactic foam core, it was helpful to evaluate the shear lag model considering only the planar half of the laminate (Figure 6) because of the symmetry of the layup. The mid-plane distorted in reverse to the facesheets (Figure 6).

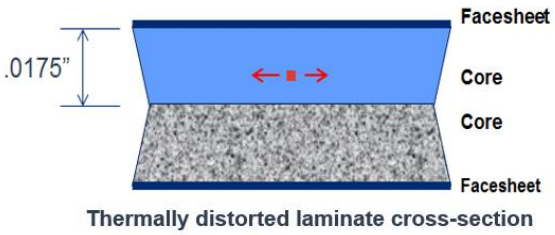

Figure 6: The Syntactic Foam Core as an Adhesive

In this evaluation of the top half of the laminate above, the facesheet was the top adherend, the top half of the syntactic foam core was the adhesive, and the bottom half of the laminate was the bottom adherend.

For the case of a 0.5-in length laminate undergoing a temperature change of -207°F (-115°C, from 20°C to -95°C), the thermal stress in the syntactic foam core at the edge of the laminate was calculated to be 1086 psi (Figure 8).

Syntactic foam SF5	
shear modulus of adhesive (psi)	145033
thickness of adhesive (in)	0.0175
M55J	
adherand 1 E (psi)	14200000
adherand 1 thickness (in)	0.011
adherand 1 CTE (in/in/F)	-2.80E-07
Midplane of SF5 core	
adherand 2 E (psi)	420595
adherand 2 thickness (in)	0.0285
adherand 2 CTE (in/in/F)	1.70E-05
initial temperature (F)	68
end temperature (F)	-139
temperature delta (F)	-207
length of joint (in)	0.5

Figure 7: Shear Lag Inputs for 0.5-in Laminate

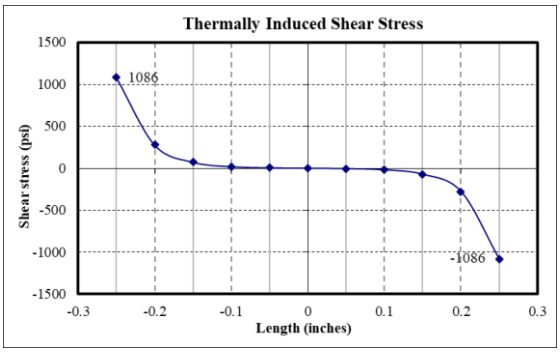

Figure 8: Shear Stress Profile of the SF in the 0.5-in Laminate based on Shear Lag Calculations

From FEA of the half-inch coupon, the shear stress at the edge of the syntactic foam was determined to be 1049 psi (Figure 9), which was within 5% of the shear lag calculation.

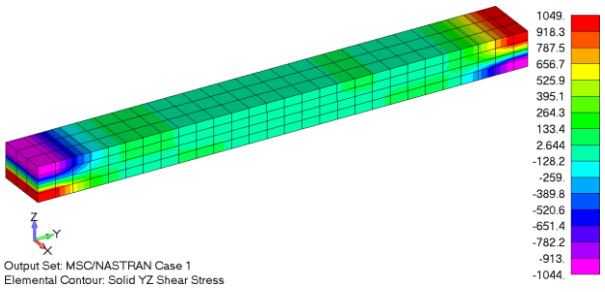

Figure 9: Shear Stress Contours of SF in the 0.5-in Laminate based on FEA

Thermal distortion loads related to CTE mismatches begin to become a problem when the length along the mismatch of the mating parts are significantly long, inducing large strains in the weaker part. The syntactic foam has a shear strength of 2520 psi.[4] At 0.5-in length, the analytical shear stress in the foam core of the substrate was 1049 psi, more than 2x under the shear stress limit. The concern for this SA substrate was that it is long at 17.5 in, and the CTE mismatch between the facesheets and core would induce stresses overcoming the shear strength of the syntactic foam.

Running the shear lag calculations and the FEA simulation of a 1-in coupon (Figure 10 and Figure 11) and a 1.5-in coupon (Figure 12 and Figure 13), the results demonstrated a remarkable contribution of the lag in the shear. The peak shear stress occurred at the edge of the coupon, and the shear dropped off almost immediately away from the edge. Also, the shear stress was seen as dependent on the thicknesses of the adhesive (core) and the adherends, not dependent on the length of the joint. The shear stress was the same at 1086 psi for all 3 lengths of coupons.

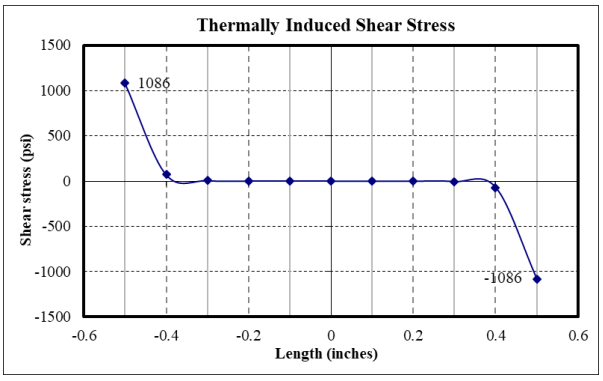

Figure 10: Shear Stress Profile of the SF in the 1.0-in Laminate based on Shear Lag Calculations

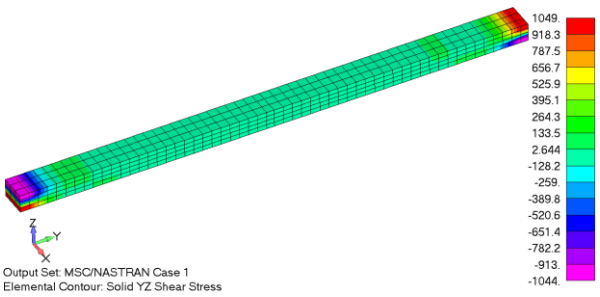

Figure 11: Shear Stress Contours of SF in the 1.0-in Laminate based on FEA

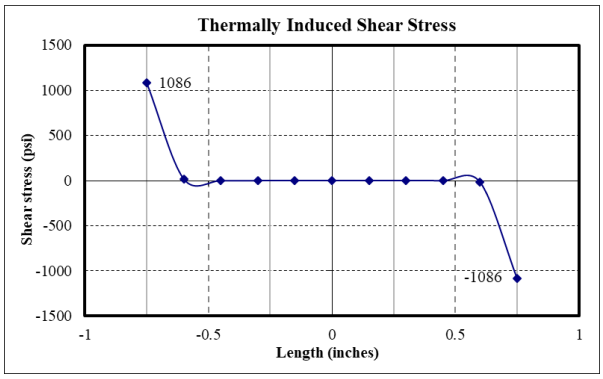

Figure 12: Shear Stress Profile of the SF in the 1.5-in Laminate based on Shear Lag Calculations

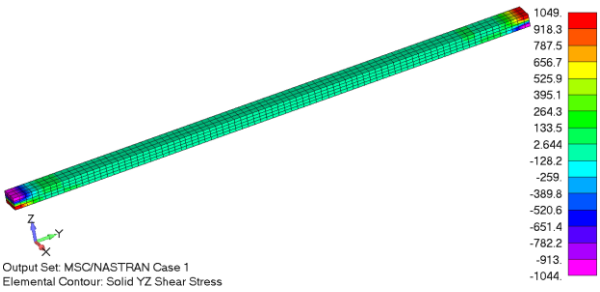

Figure 13: Shear Stress Contours of SF in the 1.5-in Laminate based on FEA

Thermal Testing Revisited

Relating these findings back to the 3 thermal tests that were conducted, the shear stresses that resulted in those tests can be surmised with justification based on testing, theoretical calculations and analytical models.

- ***Liquid nitrogen test***

The temperature of liquid nitrogen is -198°C. With this temperature change, the shear stress in the syntactic foam core was evaluated to be 2060 psi (Figure 14).

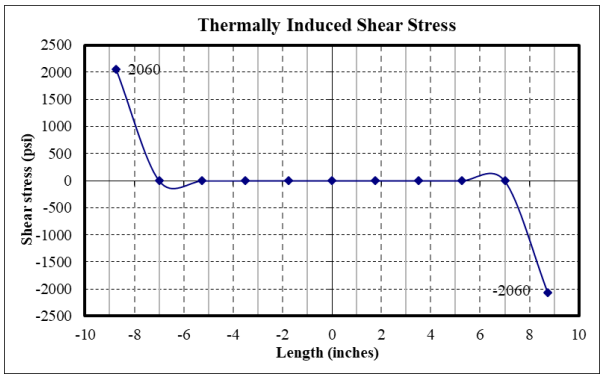

Figure 14: Shear Stress Profile of the SF in the 17.5-in Laminate after Exposure to Liquid Nitrogen

This stress was lower than the shear stress limit of 2520 psi by 1.2x, and no delamination was observed in the substrate. This was only a reference test and analysis since no mechanical testing (3-point bend) was done on specimens exposed to this temperature, and the liquid nitrogen soak was done for only one specimen with only a visual inspection for pass-fail check.

- ***3-point bend test after exposure to -150°C***

The test coupons were temperature cycled 6x at a range of -150°C to 173°C and thereafter tested in a 3-point bending configuration (as discussed in *Flexural* and *3-Point Bend* above). There were no failures in the specimens after the temperature exposure. The effect of the temperature differential from 20°C to -150°C was evaluated in the shear lag model and the shear stress in the syntactic foam was found to be 1606 psi (Figure 15), a factor of 1.6 lower than the shear allowable.

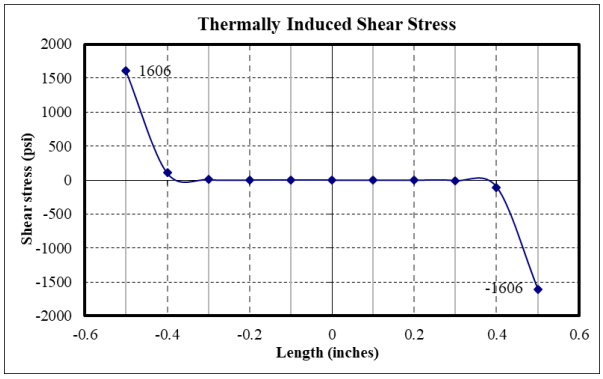

Figure 15: Shear Stress Profile of the SF in the 1.0-in Laminate after Exposure to -150°C

- ***3-point bend test after exposure to -95°C***

The test coupons were temperature cycled 6x at a range of -95°C to 105°C and thereafter tested in a 3-point bending configuration (as discussed above). No failures were observed in the specimens after the temperature exposure. The effect of the temperature differential from 20°C to -95°C was evaluated in the shear lag model and the shear stress in the syntactic foam was found to be 1086 psi (Figure 10), a factor of 2.3 lower than the shear allowable.

Confidence in Laminate

With the testing done, supported by the analyses, there was a high level of confidence that the substrate fabricated from M55J/RS3C facesheets and SF5 core would provide sufficient strength and structural integrity in the environments specified. The concerns of the foam core disintegrating and delaminating in orbit were mitigated through these component level tests and analyses.

PANEL THERMAL DEFLECTION TESTING

In keeping with the scheme of compactness in packaging, the electrical circuit that routes through and along the substrate to serve the solar cells was designed as a flexible film that bonds onto the substrate. The thickest portion of the film where most of the printed copper resided was approximately 0.0055 in. A film transfer adhesive, 3M F9460, was used to attach the flexible circuit onto the CF laminate. Because the flexible circuit had a high area density of copper, which has a CTE that is highly mismatched with CF and which has an elastic modulus that is comparable to the CF laminate, the configuration set up a classic distortion problem with a long array span that would make the array deflect a large amount normal to the panel.

Table 2: Mechanical Properties of Substrate and Flexible Circuit

Material	Elastic Modulus (psi)	Shear Modulus (psi)	Coeff Thermal Expansion (ppm/°F)
Kapton	370,000	138,000	11.00
Copper	16,000,000	5,957,000	9.11
3M F9460 adhesive	65	22	428.00
M55J/RS3C laminate	14,500,000	5,476,000	-0.28
SF5 syntactic foam	420,000	158,000	17.00
Loctite Ablestik 561K	630,000	235,000	47.20

The flexible circuit that was developed for this application had a buildup as shown in Figure 16. The long traces of copper in the primary and secondary circuits were printed at 50% areal density. Physically, the trace came out to a thickness of about 0.0028 inches. In FEA, the density was defined with the thickness of the copper layer, and the cross-sectional width was kept the same as the physical trace. Therefore, a 50% trace of copper in FEA was 0.0014 inches thick.

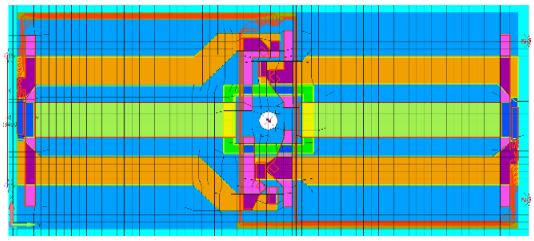

Figure 16: Buildup of the Flexible Circuit that Includes a Primary and a Secondary Circuit

The layup of the substrate and flexible circuit, including adhesive, was simulated in NASTRAN with PCOMP shell elements, where any number of individual lamina can be defined. For example, the area where there was 50% copper in the secondary circuit and nothing in the primary circuit was defined as shown in Figure 17 (thickness in inches).

Material	Thickness
11..kapton	0.001
12..copper	1.E-9
11..kapton	0.002
12..copper	0.0014
11..kapton	0.001
15..f9460 at 20C	0.002
7..m55j/rs3c (0/45/90/-45)	0.011
6..sf5	0.035
7..m55j/rs3c (0/45/90/-45)	0.011

Figure 17: 50% Copper in Secondary Circuit as Defined in NASTRAN

And in the area of the flexible circuit where there was no copper, the layup is as shown in Figure 18.

Material	Thickness
11..kapton	0.001
12..copper	1.E-9
11..kapton	0.002
12..copper	1.E-9
11..kapton	0.001
15..f9460 at 20C	0.002
7..m55j/rs3c (0/45/90/-45)	0.011
6..sf5	0.035
7..m55j/rs3c (0/45/90/-45)	0.011

Figure 18: No Copper Area as Defined in NASTRAN

For continuity in the laminate, and so that there was no stress singularity in the model, every area had a PCOMP with 9 layers. In situations where there were none of a particular material, the layer was defined with a very low thickness (1.0e-9 inches) as illustrated in Figure 18.

It was predicted that the wing assembly with the flexible circuit would deflect approximately 18 inches towards the flexible circuit side of the substrate in a cold environment defined at -95°C (Figure 20).

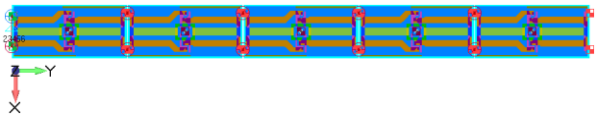

Figure 19: Wing Array FEA with Flexible Circuits

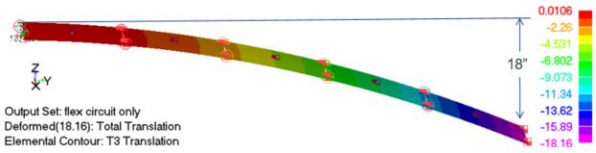

Figure 20: FEA Prediction of Wing Array Deflection

With the assumption that testing one panel with the same boundary conditions would provide a qualitative verification of the prediction, a flexible circuit was bonded to a substrate panel and thermally tested with one end clamped and the other end free, similar to a deployed condition of a panel on the array. The assembly was placed in a thermal chamber, next to a control substrate that did not have a flexible circuit. The intent of the test was to cool the panels down from 25°C to -95°C, and with a video camera, capture the deflections of both panels. A technical complication caused the video camera to terminate prematurely, and the last temperature at which the camera was operational was -70°C. The ΔT during this test was -95°C (25°C to -70°C). It was found that the panel with the flexible circuit had deflected 0.64 inches while the panel without the circuit remained unmoved (Figure 21). From the FEA prediction of the SA deflection of 18 inches (Figure 20), the 1st panel (root panel) was shown to deflect 0.76 inches with a ΔT = -115°C (20°C to -95°C). When the analytical results were scaled to ΔT = -95°C, as was the condition of the test, the predicted deflection of the root panel came to 0.63 inches, which was within 2% of the test result (Figure 22).

Figure 21: Substrate with Single-Sided Flexible Circuit Deflected 0.64 in

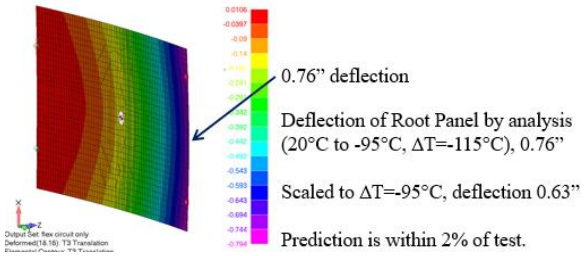

Figure 22: FEA of Test Substrate with Single-Sided Flexible Circuit Showed a Deflection of 0.63 in

It was determined that the deflection was primarily influenced by the amount of copper that was present in the laminate of flexible circuit. The driving property of copper in this deflection situation was that copper has a higher elastic modulus (16 Msi) compared to the substrate laminate (14 Msi). In addition, copper's CTE (9.1 ppm/°F) is many times higher than that of the substrate (-0.3 ppm/°F). While it may seem that the adhesive used to bond the flexible circuit onto the substrate was the influence in deflection because of its large CTE (428 ppm/°F), it has a very low elastic modulus (65 psi) – almost negligible compared to its adherents. The domination of influence in the combination of the different layers of material would come from the layer that was "stiffer" and that had relatively higher CTE than the substrate.

When CTE mismatches are working against the flatness of the substrate, there are a number of methods to overcome this. The most straightforward method is to maintain symmetry in the layup of the substrate and anything else that is being attached to that substrate. In this flexible circuit situation, another film of flexible circuit can be adhered to the substrate on the opposite face. While this creates a symmetrical, and therefore, dimensionally stable substrate, it also increases the weight of the panel and reduces the deployed modal frequencies of the array. However, just to qualify the use of symmetry to offset any deflection, the test described above was repeated with the test panel mounted with flexible circuit on its two sides. This time, both the test panel and the control panel deflections were found to be negligible at 0.01 in (Figure 23).

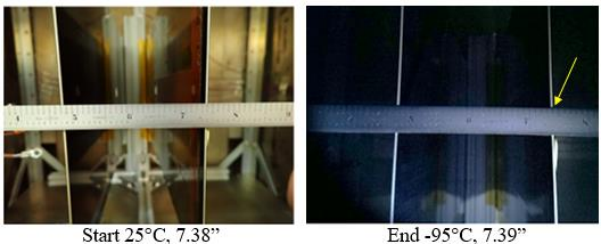

Figure 23: Substrate with Double-Sided Flexible Circuits Had No Appreciable Deflection

A lighter method to counter the effects of CTE on the flatness of a substrate is to tune a film of Kapton and the type of adhesive on the opposite side of the flexible circuit. An analysis was conducted with a layer of Kapton and another type of film adhesive to mount the Kapton. The adhesive selected, Loctite Ablestik 561K, had a significant elastic modulus to drive the counteraction against the deflection caused by the flexible circuit.

Material	Thickness
11..kapton	0.001
12..copper	0.0028
11..kapton	0.002
12..copper	0.0028
11..kapton	0.001
15..f9460 at 20C	0.002
7..m55j/rs3c (0/45/90/-45)	0.011
6..sf5	0.035
7..m55j/rs3c (0/45/90/-45)	0.011
14..ablestik 561K	0.0025
11..kapton	0.001

Figure 24: Layup with Kapton on Opposite Side of Flexible Circuit

With the layup as shown in Figure 24 it was determined that the array wing deflection was approximately 0.21 inches in the direction opposite to the flexible circuit (Figure 25). A 0.25-inch of total deflection in a run of 88 inches was considered negligible. The Kapton and adhesive layup was also considered a highly effective treatment of the substrate to counteract the tendency of the flexible circuit to distort the array. Added to the effectiveness, this method was a lighter option compared to the symmetrical layup method.

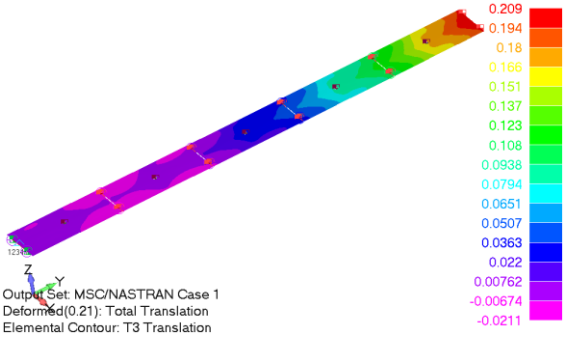

Figure 25: Wing Array with Kapton on Opposite Side of Flexible Circuit Had Negligible Deflection

DEPLOYMENT DYNAMIC SIMULATION AND LOCK-UP LOADS

To show that a free deployment was possible, the deployment dynamics of the 5-panel wing array was modeled in Adams, a dynamics simulation software. Although free deployment had the risk of high impact

loads damaging the substrate, when properly tuned, it featured less parts, weight and bulk from the elimination of a damper and a synchronizer at each hingeline, and was simpler and more reliable with less mechanisms in the assembly. The critical components in the Adams deployment simulation, other than the mass and inertia properties of the assembly, were the hinged joints for stowing and unfolding, the torsion springs for unfolding upon release actuation and the hinge latches to lock the array in the deployed state.

Hinges were modeled with Adams built-in connectors. The hinges deploy by means of torsion springs which were modeled with rotational spring-damper forces. Parts that physically bump or slide against each other were defined with the appropriate contact forces. For the bump-stops on the hinge at the fully deployed positions, the contact was tuned so that there was compliance at hinge lockup, somewhat simulating the flexibility of the wing. This also allowed for impact and rebound responses in the wing assembly, and generated lockup loads that were within the capability of the substrate.

A hinge latch was employed for each hingeline in the 5-panel array design. The latch was a thin titanium tab that hooked onto a nub when the hinges were fully deployed. The locking tab was modeled in Adams with discrete flexible links, which are essentially rigid bodies joined together with elastic beam elements. To allow the tab to ride up and latch onto the nub, contact was defined between the two parts.

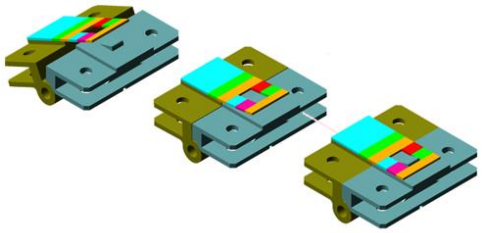

Figure 26: Progression of Hinge Deployment Featuring Locking Mechanism

To ensure that the tab stayed latched on the nub once it slid over the nub, friction between the tab and the nub had to be defined. If friction were not present, the rebound loads of the hinges at contact would cause the latching mode to reverse and unlatch.

Figure 27: Latch Tab in Preloaded State when Hinge is Fully Deployed

Hinge friction and the resistive torque of the harnesses that run across the hingelines were accounted for. The torsion spring rates were set to the same value for all hingelines, as it was determined that different spring rates in the assembly induced a disorderly unfolding of the panels. The spring rate was tuned to be higher than the hingeline resistive torques throughout the deployment. A suitable spring rate was achieved that balanced sufficient torque for deployment and sufficient kinetic energy to minimize lock-up loads. The actuation of the panel deployment was activated with a timed removal of a constraint that held the outermost panel against the other 4 panels at the cup-and-cone stowing interface. It can be seen that the array deployed in a controlled manner, moving in a steady direction that was normal to the stowed plane (Figure 28).

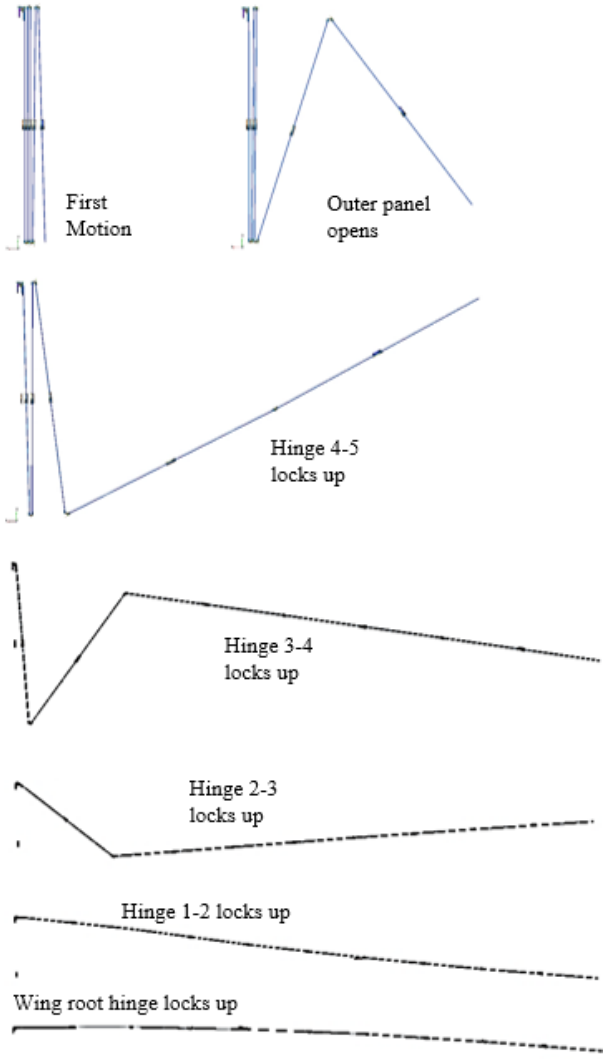

Figure 28: Progression of 5-Panel Wing Deployment

The lock-up loads recovered from the simulation show a max hinge moment of 80 in.lb (Figure 29).

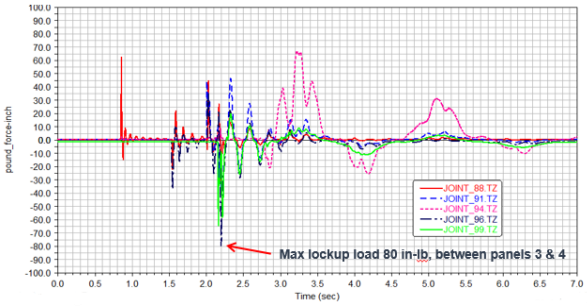

Figure 29: Torque at Wing Joints in Deployment

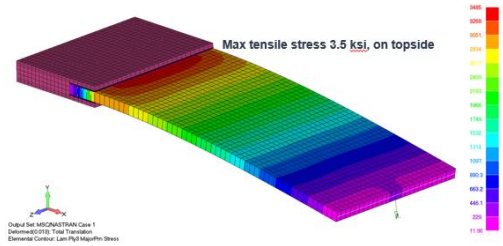

M55J/RS3C Laminate Compressive Strength	39.7	ksi
Max Stress	3.5	ksi
Factor of predicted failure	**11.34**	
width of coupon	1	in
width of hinged edge	8	in
distance from hinge to load point	2	in
moment at unit load	16	in-lb
Max moment to failure	**181.5**	**in-lb**

Figure 30: Analytical Max Failure Moment 181 in-lb

It was predicted that the *Cantilevered* test would see a max load at failure of 11.34 lb, which was within 3% of the B-basis test results of 11.6 lb. Scaling the load for the actual panel width, the max failure torque was determined to be 181 in-lb. The predicted lock-up load during deployment of 80 in-lb was well under the allowable torque of 181 in-lb, demonstrating a margin of 0.51 over a safety factor of 1.5.

VIBRATION AND DEPLOYMENT TESTING

In the progression of the Express project, an engineering model (EM) was built where the substrate laminate was made out of a single material –M55J/RS3C in a quasi-isotropic layup of $[0/45/90/-45]_{S3}$. The panels were shorter at 15 in and there were a total of 4 panels in the array assembly. The hinges, latches and launch interfaces were the same as the 5-panel array. The EM was a bare substrate assembly without the arrays, circuits, and adhesives. The EM was built to validate the design in its environments and for its functions, as a proof-of-concept. This section will not extensively cover the testing that was done, but demonstrate that a 4-panel, thin substrate, and lightweight array of similar build was vibration tested and set up to deploy.

Vibration Test

The vibration environment was a sine vibration at 15 g and a random vibration at 14.1 g RMS. The nature of the design of the foldable array was that it features unsupported panel ends and gaps between panels (Figure 31) allowing the panels to contact and rattle against each other. The assembly modal signature showed a first mode frequency of 58 Hz (Figure 33). This EM vibration test demonstrated that a flexible thin-panel assembly with unsupported ends and rattle gaps, was not out of the realm of feasibility. The assembly survived the environments that it was exposed to, and showed no degradation in structural integrity. Cantilevered panels and rattle gaps are seen to be conflicting with sound structural design, but the rattle gaps act as an energy damper, attenuating acceleration response peaks.

Figure 31: Hinged Edge Members Showing Rattle Gaps between Panels

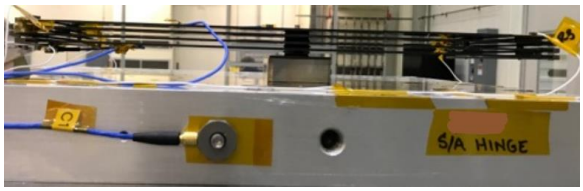

Figure 32: 4-Panel Array Vibrated in Panel-Normal Direction

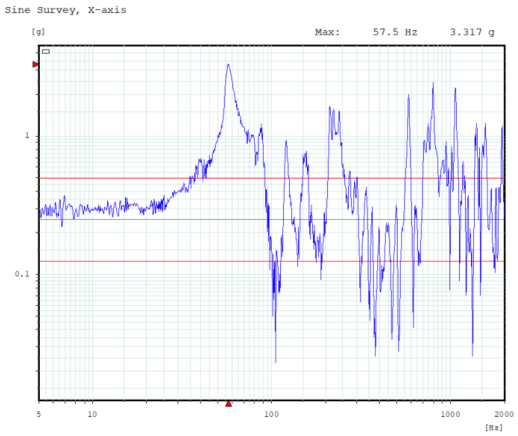

Figure 33: 4-Panel Array at 58 Hz Stowed First-Mode Frequency

Deployment Test

The 4-panel EM array was significantly different from the 5-panel array in that the first panel, or root panel, was fixed, reflecting a design intention to attach the array to a gimbal. The deployment test was rigged to maintain the root panel stationary, while the 3 subsequent panels were allowed to freely deploy. The middle of the 3 panels was suspended to a gantry system to offload some of the weight of the assembly on the panel hinges. The torsion springs were checked that they provided sufficient torque to deploy against the gantry's inertia lag and panels' wind resistance.

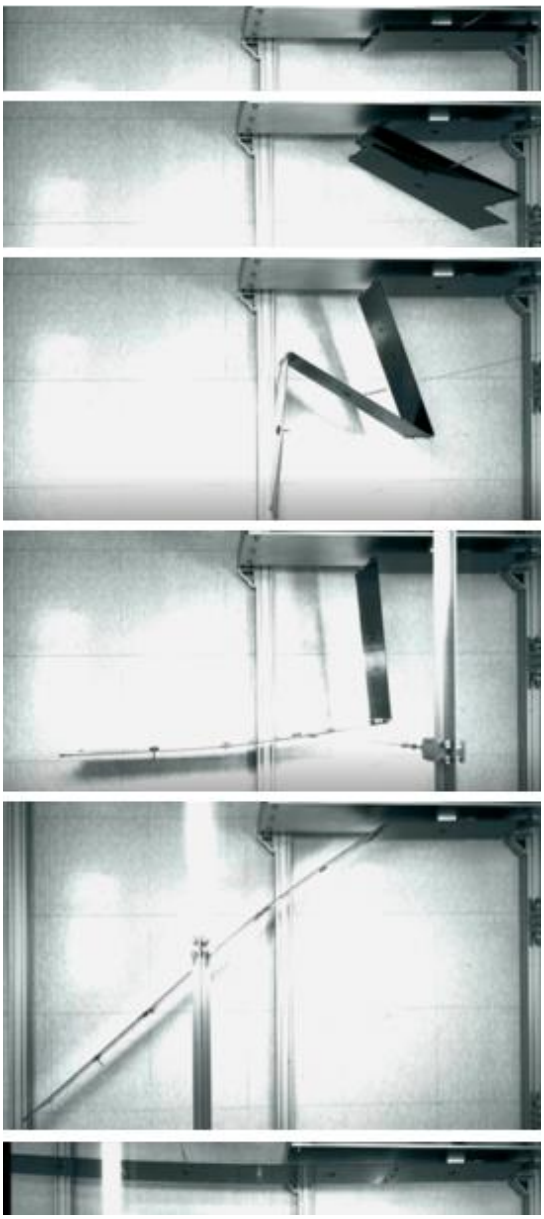

Figure 34: Deployment Progression of EM in Deployment Test

Adams Deployment Simulation

The 4-panel EM array and the gantry system were modeled in Adams to predict the behavior of the deployment. The effect of the gantry's inertia lag was introduced by a tether attached between the array and the gantry. Also, with the test conducted in air, the effects of wind resistance was modeled with a normal force on each panel that was proportional to the velocity of the panel. Additionally, gravity was introduced into the dynamics. It can be seen from Figure 34 and Figure 35 that the modes of the deployment test were identical to the Adams simulation.

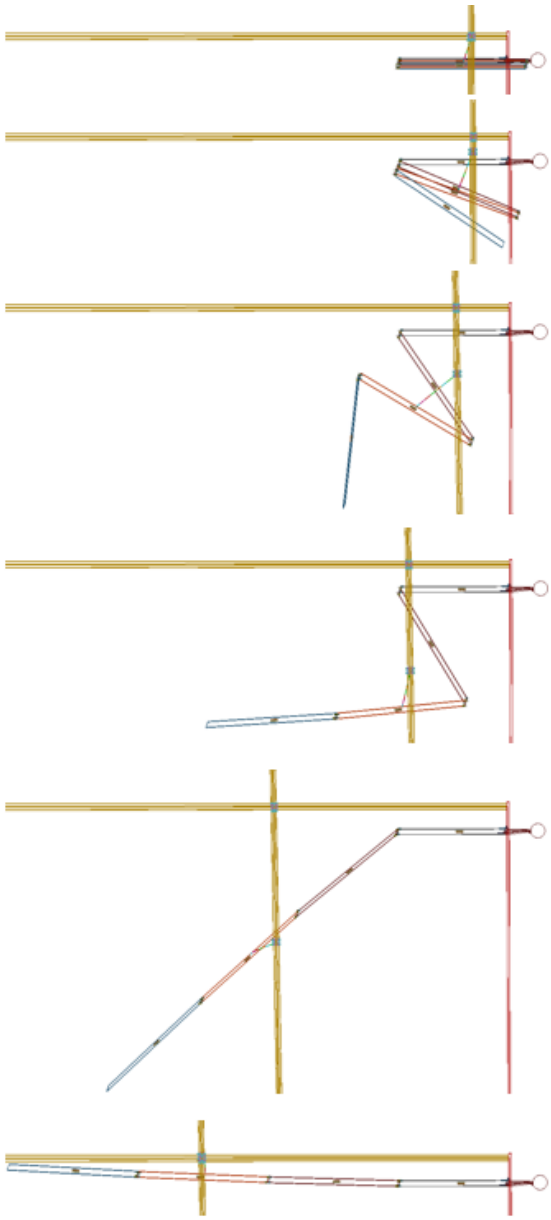

Figure 35: Deployment Progression of EM in Adams

Although the 4-panel EM deployment configuration was markedly different from what a 5-panel deployment would look like, the test proved out the hinge and latch designs, which were the same in both array designs, and showed that a free deployment was possible. It also demonstrated that with some adjustment in the hinge springs, the panels could be deployed against unpredicted resistive torques.

CONCLUSION

The development work and testing that have been done have progressively qualified the use of syntactic foam as a core material together with CF facesheets in the fabrication of thin, lightweight, and large wingspan substrates for solar arrays. The substrate has been demonstrated to be stable in thermal environments and maintained structural integrity in large temperature differentials, within operational limits. A layup with materials that have mismatched CTE can be sensibly designed such that large thermal distortions are minimized. The mechanisms testing has proven out the hinge and latch designs and the selection of torsion springs. The vibration testing thus far has set the foundation for cantilevered-panel and rattle-gap designs where the situation calls for it. The deployment testing and Adams simulations have increased confidence in this deployable array form factor.

Future work would build on what has already been developed. Mechanically, a complete test verification campaign would bring forward the thin-substrate, folded and deployable array assembly as a qualified subsystem. More detailed testing of lightweight, flexible circuits would need to be done. The interaction of solar cells on the array panels would need to be investigated and thermally and mechanically tested.

Acknowledgements

I would like to thank the following at APL: Erich Schulze for his mechanical expertise and for managing the substrate manufacturing and testing program; Mark Bryant for his technical oversight and resourcefulness in the substrate and wing array efforts; Ken Harclerode whose designs transform concept to reality; Michael Marley for his leadership in steering the project and the environmental requirements; Paul Wienhold and Ryan Quinn for their composites expertise in fabricating the substrate; Michael Butler and Carson Baisden for leading the flexible circuit effort; David Persons for his wisdom and guidance; Clint Apland for his game in mechanisms and direction in this development; and James Leary for his support and leadership on this program that allowed for this valuable work to be done. Thanks to Tencate Advanced Composites for providing additional CTE information on their syntactic foam. All the work that was accomplished in this development and testing was funded by a small-satellite program at APL.

References

1. Apland, C., Rogers, A., Persons, D., Summers, R., and Kee, L. “A Flexible Rideshare Adapter System to Increase Space Access for Express Class 20-50 kg Small Satellite Missions.” 27th Annual AIAA/USU Conference on Small Satellites, Logan, UT, 2013.
2. Apland, C., Kee, L., and Rogers, A. “Release System for Deploying Satellites.” U.S. Patent 10,053,243 B2, issued August 21, 2018.
3. Volkersen, O. “Die Nietkraft Verteilung in Zugbeanspruchten Nietverbindungen mit Konstanten Laschenquerschnitten.” Luftfahrtforschung, 15 (1938), pp. 41-47
4. Tencate Advanced Composites “SF-5 Syntactic Film.” Product Data Sheet, 2015.